Available online at www.sciencedirect.com

SciVerse ScienceDirect

Ceramics International 39 (2013) 7343–7353

CERAMICS INTERNATIONAL

www.elsevier.com/locate/ceramint

The improvement of electron transport rate of TiO_2 dye-sensitized solar cells using mixed nanostructures with different phase compositions

A.M. Bakhshayesh, M.R. Mohammadi*

Department of Materials Science and Engineering, Sharif University of Technology, Azadi Street, Tehran, Iran

Received 22 December 2012; received in revised form 9 January 2013; accepted 22 February 2013
Available online 1 March 2013

Abstract

Dye-sensitized solar cells (DSCCs) in the form of mixed nanostructures containing TiO_2 nanoparticles and nanowires with different weight ratios and phase compositions are reported. X-ray diffraction and field emission scanning electron microscopy analyses revealed that the synthesized TiO_2 nanoparticles had average crystallite size in the range 21–39 nm, whereas TiO_2 nanowires showed diameter in the range 20–50 nm. The indirect optical band gap energy of TiO_2 nanowires, anatase- and rutile-TiO_2 nanoparticles was calculated to be 3.35, 3.28 and 3.17 eV, respectively. The power conversion efficiency of the solar cells changed with nanowire to nanoparticle weight ratio, reaching a maximum at a specific value. An increase of 4.3% in cell efficiency was achieved by introducing 10 wt% nanowire into the as-synthesized TiO_2 nanoparticles (WP1 cell). Furthermore, an increase of 27.6% in cell efficiency was achieved by using crystalline anatase-TiO_2 nanoparticles rather than as-synthesized TiO_2 nanoparticles in WP1 solar cell. It was found that the power conversion efficiency and short circuit current of WP1 cell were decreased down to around 30.8% and 39.1%, respectively using rutile nanoparticles rather than anatase nanoparticles. The improvement of cell efficiency was related to rapid electron transport and less recombination of photogenerated electrons, as confirmed by electrochemical impedance spectroscopy.

Keywords: A. Sol–gel processes; C. Electrical properties; D. TiO_2; Dye-sensitized solar cell

1. Introduction

Recently, dye-sensitized solar cells (DSSCs) have been regarded as a promising candidate for third solar cells generation owning to their ease of manufacturing, good power conversion efficiency, low cost, optional high vacuum and materials purification steps compared with p–n junction photovoltaic devices. The mesoporous films made of 20 nm diameter particles are characterized by power conversion efficiency exceeding 12% [1–3]. Following excitation by sunlight, the dye molecules inject electrons in the TiO_2 conductive band and holes in the electrolyte. The conduction mechanism of dye-sensitized solar cells is based on majority carrier transport despite the minority carrier transport of conventional p–n junction in organic solar cells [4,5]. In order to reach high conversion efficiencies for the DSSCs, it is important to collect these photogenerated charge carriers as electric current before they recombine. To achieve this goal, the charge carrier collection has to be significantly faster than their recombination. However, DSSCs made of nanoparticles, rely on limited diffusion for electron transport; a slow mechanism that can limit device efficiency, especially at longer wavelengths. One promising solution to this impasse is to increase the electron diffusion length in the photoanode by replacing the nanoparticle film with one-dimensional TiO_2 such as nanowires [6], nanotubes [7] and nanobelts [8]. Generally, high electron mobility, excellent electron–hole separation power and long-distance transport ability are unique advantages of one-dimensional TiO_2 compared to that of bulk TiO_2 [9,10]. However, the insufficient surface area of one-dimensional nanostructures constrains the power conversion efficiency to relatively low levels in order of 1–2% [6,11]. In order to use nanowires and nanoparticles advantages simultaneously, TiO_2 solar cells in the form

*Corresponding author. Tel.: +98 21 6616 5211; fax: +98 21 6600 5717.
E-mail addresses: mrm41@cam.ac.uk, mohammadi@sharif.edu (M.R. Mohammadi).

0272-8842/$ - see front matter © 2013 Elsevier Ltd and Techna Group S.r.l. All rights reserved.
http://dx.doi.org/10.1016/j.ceramint.2013.02.073

of mixed nanostructures composed of a mixture of one-dimensional TiO_2 nanostructures and nanoparticles with various weight ratios have been reported. Asagoe et al. [12] reported that the DSSC made of 10 wt% anatase nanowire and 90 wt% P-25 nanoparticle showed higher photovoltaic performance (with power conversion efficiency of 6.53%) than the DSSC made of pure P-25 nanoparticle (with power conversion efficiency of 5.59%). Tan and Wu [13] fabricated dye-sensitized solar cells based on nanoparticle/nanowire composite films and investigated effect of nanowire to nanoparticle weight ratio on their performance. They found that a mixture of 20 wt% nanowire and 80 wt% nanoparticle had the maximum power conversion efficiency of 8.6%. The similar results have been reported by Su et al. [14] as well. Pan et al. [15] prepared dye-sensitized solar cells based on P-25 nanoparticle and nanobelt composite films with different weight ratios. The results revealed that the composite film containing 2 wt% nanobelt showed the highest cell efficiency of 6.96%. Lee et al. [16] studied photovoltaic performance of a DSSC containing mixtures of TiO_2 nanoparticles and nanotubes synthesized by the sol–gel and hydrothermal methods, respectively. The cell efficiency of mixed nanostructures containing 0 wt%, 10 wt% and 20 wt% nanotubes was measured to be 3.84%, 4.57% and 4.07%, respectively. Pavasupree et al. [11] reported that photoanode electrode made of a mixture of TiO_2 nanorods and nanoparticles, synthesized by hydrothermal process, had higher power conversion efficiency than that made of pure nanoparticles. So far, no significant work has been studied on the influences of nanowire to nanoparticle weight ratio on the internal resistances, electron lifetime and electron transit time of TiO_2 DSSCs.

In the present work, a new formulation of TiO_2 paste was developed for fabrication of DSSCs composed of mixtures of synthesized nanoparticles and nanowires. Electron transport improvement of TiO_2 DSSCs was achieved by using mixed nanostructures. In addition, the influences of nanowire to nanoparticle weight ratio and phase composition of the nanoparticles on photovoltaic characteristics of fabricated DSSCs were studied. The improvement mechanism of DSSCs was investigated by measurement of their internal resistances, electron lifetime and electron transit time using electrochemical impedance spectroscopy (EIS).

2. Experimental

2.1. Preparation of anatase-TiO_2 nanowires

TiO_2 nanowires were grown by a two consecutive hydrothermal operation. Hydrogen titanate nanowires were firstly prepared by hydrothermal process according to an analogous procedure reported in the literature [17]. Hydrogen titanate nanowires were then converted into TiO_2 nanowires by a rehydrothermal process. In the first step, 1 g TiO_2 powder (anatase, Alfa Aesar, 99%) was placed into 47 ml Teflon-lined stainless steel autoclave, which was then filled with 10 M NaOH aqueous solution up to 80% of the total volume. The autoclave was heated at 180 °C for 48 h and subsequently cooled naturally to room temperature. The collected precipitates (i.e., hydrogen titanate nanowires) were washed with dilute HCl and water several times and dried at 25 °C. In the second step, hydrogen titanate nanowires were placed into the Teflon-lined autoclave, which was then filled with deionised water (pH = 7) up to 80% of the total volume. The autoclave was heated at 180 °C for 12 h and subsequently cooled to room temperature naturally. Finally, the resulting TiO_2 nanowires were collected and dried at room temperature.

2.2. Preparation of TiO_2 nanoparticles

TiO_2 nanoparticles were prepared by particulate sol–gel process according to our previous study [18]. Titanium tetraisopropoxide (TTIP) with a purity of 97% (Aldrich, UK) was used as a titanium precursor; analytical grade hydrochloric acid (HCl) 37% (Fisher, UK) was used as a catalyst for the peptisation and deionised water was used as a dispersing media. The water–acid mixture (pH = 2) was stabilised at a constant temperature. TTIP was added, forming a white thick precipitate, which was gradually peptised after 2 h to form a clear sol. The molar ratio of TTIP:HCl:H_2O was 0.1:0.06:50, which makes a 0.1 M TiO_2 sol. As-synthesized TiO_2 nanoparticles were prepared by heating the sol at 70 °C for 24 h. Since the as-synthesized nanoparticles had almost crystalline anatase structure, they were treated in two different methods in order to obtain highly crystalline anatase and rutile structures. They were annealed at 900 °C for 2 h to obtain crystalline rutile nanoparticles, whereas they were treated by hydrothermal process using deionised water (pH = 7) at 230 °C for 8 h to obtain crystalline anatase nanoparticles.

2.3. Preparation of DSSCs

Basically, two categories of TiO_2 DSSCs were fabricated in order to study the effect of nanowire to nanoparticle (W:P) weight ratio and phase composition of the nanoparticles on cell performance, as shown in Table 1. The first category consisted of seven different TiO_2 pastes with various W:P (i.e., anatase nanowires to as-synthesized nanoparticles) weight ratios. The optimal W:P weight ratio was determined from the photovoltaic performance of fabricated DSSCs. The second category consisted of two different TiO_2 pastes with various nanoparticle phase compositions (i.e., crystalline anatase and rutile phases). A new formulation of TiO_2 paste was developed in our lab. Both categories of TiO_2 pastes were prepared by mixing the synthesized nanowires and nanoparticles, the solvent, the dispersing agents and binders. One solar cell was also fabricated from commercial TiO_2 powder as a reference (called commercial cell) to compare with the rest of fabricated solar cells.

Table 1
Characteristics of fabricated TiO_2 dye-sensitized solar cells.

	Category I						Category II	
	Effect of W:P weight ratio using the as-synthesized nanoparticles						Effect of nanoparticle phase composition for WP1 cell	
W:P	0:100	10:90	20:80	30:70	40:60	50:50	100:0	Anatase phase	Rutile phase
DSSC	P	WP1	WP2	WP3	WP4	WP5	W	WP1A	WP1R

TiO_2 monolayer films were coated on FTO (15 Ω/sq) substrate by spin coating technique using a Pasargad Nanotechnology spin coater. The deposited TiO_2 films with thickness around 14 μm, as photoanode electrodes, were sintered at 500 °C for 2 h in air atmosphere. The post-treatment with $TiCl_4$ solution was applied to freshly sintered TiO_2 electrodes as reported in the literature [19]. An aqueous stock solution of 2 M $TiCl_4$ was diluted to 0.04 M. TiO_2 electrodes were immersed into the solution and stored in an oven at 70 °C for 30 min in a closed vessel. After flushing with distilled water, the electrodes were sintered again at 450 °C for 30 min. The resulting TiO_2 electrodes were soaked in 0.5 mM ruthenium (II) dye (Ruthenium 535-bisTBA dye, or N719, Solaronix) solution (using ethanol as a solvent) for 18 h. The electrodes were washed with ethanol, dried and then immediately used for photovoltaic measurements.

The redox electrolyte was composed of 0.6 M dimethylpropylimidazolium iodide, 0.1 M LiI, 0.05 M I_2, and 0.5 M 4-tertbutylpyridine in acetonitrile [20]. Platinum coated FTO substrate, with a small hole, was prepared as a counter electrode. The Platinum electrode was placed over the dye-adsorbed TiO_2 electrode, and the edges of the cell were sealed with sealing sheet (SX 1170-60, Solaronix). Sealing was accomplished by hot-pressing the two electrodes together at 120 °C. The redox electrolyte was injected into the cell through the small hole of the counter electrode and sealed with a small square of sealing sheet.

2.4. Characterization and measurements

TiO_2 photoanode electrodes were characterized by X-ray diffraction diffractometer (XRD) using a Philips X'pert PW3020, Cu-K_α and field emission scanning electron microscope (FE-SEM) using a JEOL 6340. The thickness of TiO_2 electrodes was measured with a Tensor Alpha-step Profiler. The absorption spectrum was analyzed by Ultraviolet–visible (UV–vis) spectroscopy using a 6705 JENWAY spectrometer. The density of TiO_2 nanostructures was measured by a Micromeritics AccuPyc 1330 pycnometer analyzer. They were also characterized in specific surface area and pore volume by nitrogen absorption, from Brunauer–Emmett–Teller (BET) and Barret–Joyner–Halenda (BJH) equations, respectively at 77.35 K using a Micromeritics Tristar 3000 analyzer. External surface area of the samples was calculated by De-Boer equation [21]. Prior to BET measurement, powders were degassed for 20 h at 100 °C with pressure of 0.1 Pa. Photovoltaic measurements were performed under 1 Sun AM 1.5G using Luzchem simulated sunlight. The electrochemical impedance spectroscopy (EIS) measurements of the DSSCs were recorded with a potentiostat/galvanostat (PGSTAT 302N, Autolab, Eco-Chemie, the Netherlands) under 100 mW/cm^2. The frequency range was explored from 0.01 Hz to 10^6 Hz. EIS spectra were simulated using Zview software.

3. Results and discussion

3.1. Microstructure

Fig. 1 shows surface morphology of deposited TiO_2 photoanode electrodes. It is evident that the deposited films had uniform, homogeneous and porous structure as a result of removal of the dispersing agents, binders and solvents. The electrodes were uniformly covered with different weight ratios of TiO_2 nanowires and nanoparticles. TiO_2 nanowires had length of several μm and diameter in the range 20–50 nm, whereas TiO_2 nanoparticles showed diameter in the range 21–39 nm. As can be observed, the porosity of deposited films depends on nanowire to nanoparticle weight ratio since TiO_2 nanoparticles were settled down between the porosity of TiO_2 nanowires. Defects (i.e., porosity) in the deposited films may act as electron traps. The depth of the traps that participate in the electron motion affects the value of the diffusion coefficient [22]. Moreover, TiO_2 nanoparticles usually have higher surface area than TiO_2 nanowires. This is an essential parameter for a high-efficient DSSC, because it allows adsorption of sufficiently large number of dye molecules needed for efficient light harvesting. Consequently, the cell efficiency of TiO_2 electrodes containing pure nanowires is expected to be improved by introducing TiO_2 nanoparticles in the form of mixed nanostructures.

3.2. Crystal structure

Fig. 2 shows XRD patterns of prepared nanostructures. Basically, the as-grown nanowires prepared by one step hydrothermal process consisted of hydrogen titanate phase ($H_2Ti_3O_7$) rather than anatase-TiO_2 phase (Fig. 2a). Formation mechanism of hydrogen titanate during hydrothermal process can be explained by the following reactions [23]:

$$3TiO_2 + 2NaOH \rightarrow Na_2Ti_3O_7 + H_2O \quad (1)$$

$$Na_2Ti_3O_7 + 2HCl \rightarrow H_2Ti_3O_7 + 2NaCl \quad (2)$$

We found that hydrogen titanate nanowires can be converted into TiO_2 nanowires by a rehydrothermal process in presence of deionised water. Therefore, a two consecutive hydrothermal operation was employed to produce TiO_2 nanowires. The rehydrothermally grown nanowires and nanoparticles treated by hydrothermal process had crystalline anatase structure with the strongest peak at $2\theta = 25.3^\circ$ (1 0 1), whereas nanoparticle sintered at 900 °C showed crystalline rutile structure with the strongest peak at $2\theta = 27.4^\circ$ (1 1 0). The broad peaks indicated that ultra-fine primary particles were obtained. The average crystallite size of crystalline anatase and rutile nanoparticles was calculated to be around 18 nm and 24 nm,

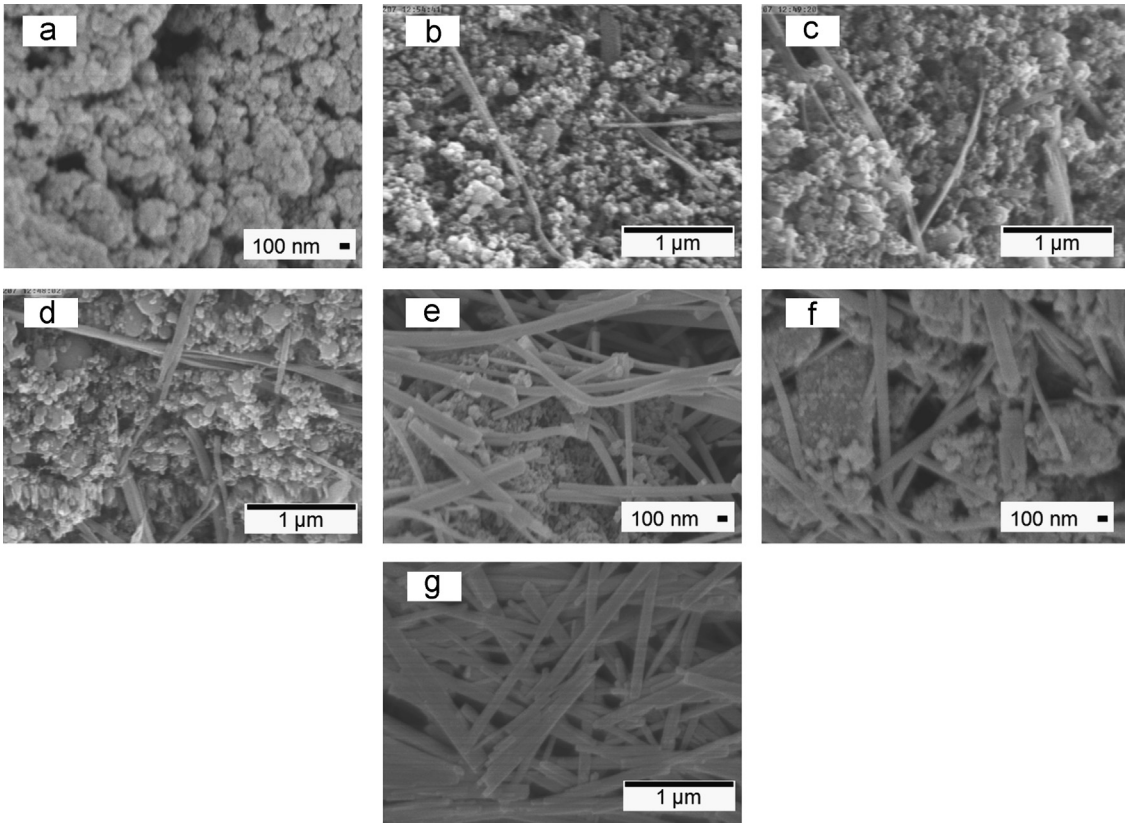

Fig. 1. FE-SEM images of surface morphology of TiO_2 photoanode electrodes: (a) P, (b) WP1, (c) WP2, (d) WP3, (e) WP4, (f) WP5 and (g) W.

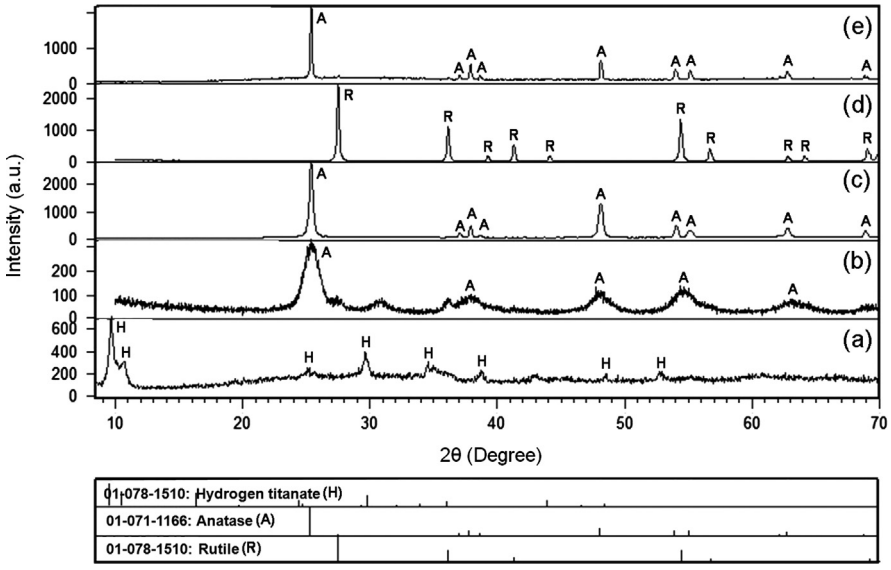

Fig. 2. XRD patterns of prepared nanostructures: (a) hydrothermally grown nanowires ($H_2Ti_3O_7$), (b) as-synthesized nanoparticles (with almost crystalline anatase structure), (c) nanoparticles treated by hydrothermal process (with crystalline anatase structure), (d) nanoparticles annealed at 900 °C (with crystalline rutile structure) and (e) rehydrothermally grown nanowires (with crystalline anatase structure). H: Hydrogen titanate, A: anatase-TiO_2 and R: rutile-TiO_2.

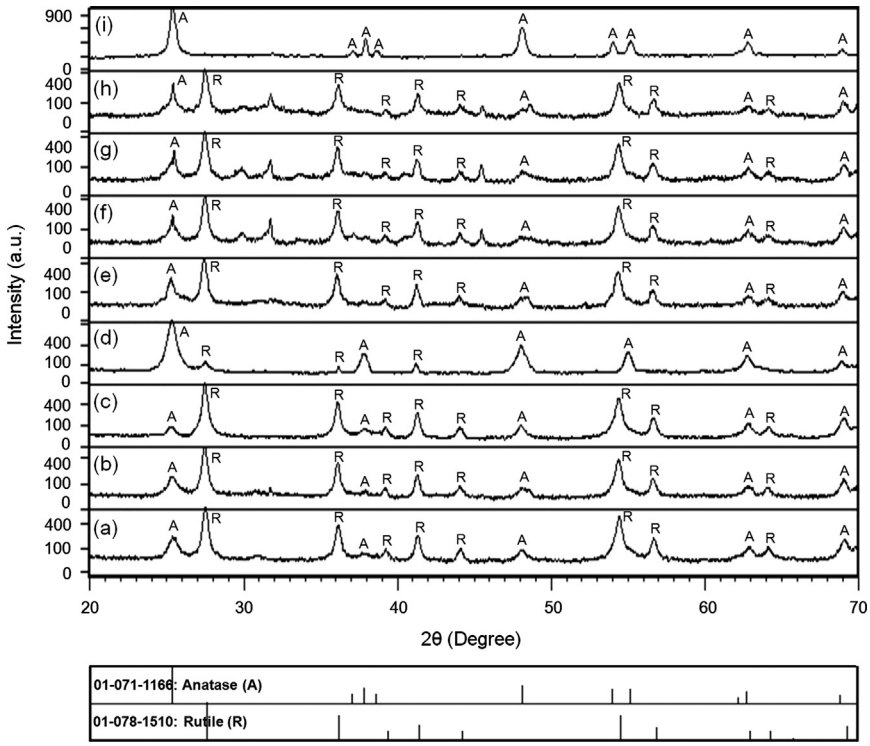

Fig. 3. XRD patterns of 500°C annealed TiO_2 photoanode electrodes: (a) P, (b) WP1, (c) WP1R, (d) WP1A, (e) WP2, (f) WP3, (g) WP4, (h) WP5 and (i) W. A: anatase-TiO_2 and R: rutile-TiO_2.

respectively by the Scherrer equation as follows [24]:

$$d = \frac{k\lambda}{B\cos\theta} \tag{3}$$

where d is the crystallite size, k is a constant of 0.9, λ is the X-ray wavelength of Cu which is 1.5406 A°, θ is the Bragg angle in degree, and B is the full width at half maximum (FWHM) of the peak.

Fig. 3 shows XRD patterns of 500 °C annealed TiO_2 photoanode electrodes in the form of mixed nanostructures containing TiO_2 nanowires and as-synthesis nanoparticles. It can be observed that W had anatase structure with the strongest peak at $2\theta = 25.3°$ (1 0 1) (Fig. 3i),

whereas other electrodes showed a mixture of anatase and rutile phases by dominant peaks at $2\theta = 25.3^\circ$ (1 0 1), and $2\theta = 27.4^\circ$ (1 1 0), respectively (Fig. 3a–h). Since the brookite content is negligible at temperatures higher than 500 °C, the mass fraction of rutile (X_R) in the crystal lattice can be calculated based on the relationship between the integrated intensities of anatase (1 0 1) and rutile (1 1 0) peaks by the following formula developed by Spurr and Myers [25]:

$$X_R = \frac{1}{1 + K(I_A/I_R)} \quad (4)$$

where I_A and I_R are the integrated peak intensities of the anatase and rutile peaks, respectively. The empirical constant K was determined via XRD powders analyses of known proportions of pure anatase and pure rutile TiO_2, and is equal to 0.79. The mass fraction of anatase and rutile phases as well as their average crystallite size is shown in Table 2. It is evident that, anatase content of mixed nanostructure films was increased with increasing nanowire to nanoparticle weight ratio. This can be related to the phase composition of nanowires and nanoparticles, being pure anatase and a mixture of anatase and rutile phases, respectively. Moreover, the average crystallite size of deposited electrodes was decreased with an increase of nanowire to nanoparticle weight ratio. There is more supporting evidence in favour of anatase as the most promising for solar cell application [26]. However, as mentioned in the Introduction section, TiO_2 nanoparticles have higher dye sensitization capability than the nanowires due to possessing higher surface area. Consequently, it is expected an optimum weight ratio of nanowire to nanoparticle shows the best photovoltaic performance.

3.3. BET analysis

Fig. 4 illustrates the N_2 adsorption–desorption isotherms of prepared TiO_2 nanoparticles and nanowires. N_2 adsorption characteristics of the nanostructures were also summarized in Table 3. TiO_2 nanoparticles had higher surface area than TiO_2 nanowires, resulting in large adsorption of dye molecules on the surface of nanoparticles. As expected, surface area of the as-synthesized nanoparticles reduced drastically, while their pore volume and pore size increased after annealing at 500 °C. Therefore, the as-synthesized nanoparticles showed the highest surface area (i.e., 154 m^2/g) amongst all nanostructures.

3.4. UV–vis analysis

Optical absorbance spectra of TiO_2 nanowires and nanoparticles are shown in Fig. 5. It has been reported that bulk rutile has a direct band gap of 3.06 eV and an indirect band gap of 3.10 eV, while bulk anatase only shows an indirect band gap of 3.23 eV [27–29]. To quantify the optical band gap of the films, Tauc Model [30] was employed in the high absorbance region of the transmittance spectra according to the following equation:

$$\alpha h\nu = A(h\nu - E_g)^r \quad (5)$$

where $h\nu$ is the photon energy, E_g is the optical band gap, A is a constant which does not depend on photon energy, r has four numeric values (1/2 for allowed direct, 2 for allowed indirect, 3 for forbidden direct and 3/2 for forbidden indirect optical transitions) and α is the absorption coefficient which is calculated from the following equation:

$$\alpha = \frac{2.303K\rho}{LC} \quad (6)$$

where K is the absorbance of the sample; ρ is the density of TiO_2 nanostructure; C is the concentration of the particles

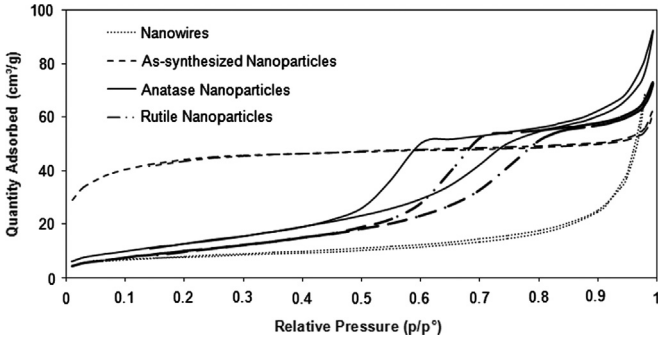

Fig. 4. Nitrogen adsorption–desorption isotherm of prepared TiO_2 nanostructures.

Table 2
The percentage of anatase and rutile phases of deposited TiO_2 photoanode electrodes.

	Anatase (%)	Rutile (%)	Crystallite size (nm)
P	36.6	63.4	35.4
WP1	42.9	57.1	33.1
WP2	49.3	50.7	31.5
WP3	55.6	44.4	30.2
WP4	62.0	38.0	28.8
WP5	68.3	31.7	27.9
W	100	0	22.4
WP1A	72.2	27.8	20.0
WP1R	36.9	63.1	39.7

Table 3
N_2 adsorption characteristics of TiO_2 nanostructures.

Sample	S_{BET} (m^2/g)	$S_{Ext.}$ (m^2/g)	$V_{Tot.}$ (cm^3/g)	P (nm)
As-synthesized nanoparticles	154.5	78.6	0.083	02.1
Anatase nanoparticles	49.3	64.5	0.111	09.0
Rutile nanoparticles	39.2	54.2	0.096	09.8
As-grown nanowires	29.4	21.9	0.106	14.5

S_{BET}: BET specific surface area; $S_{Ext.}$: external surface area calculated from t-method by D-Boer equation; $V_{Tot.}$: total pore volume calculated by BJH method; P: pore size calculated by BJH method.

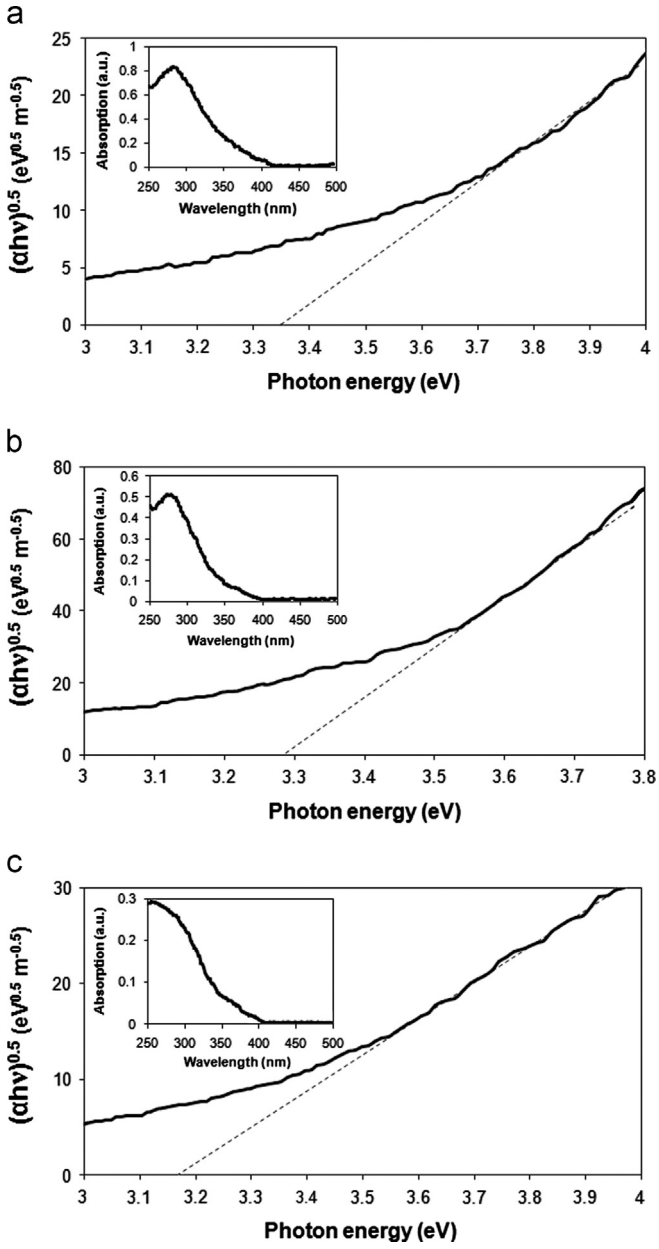

Fig. 5. Optical absorbance spectra and the plots of $(\alpha hv)^{0.5}$ versus photon energy of: (a) TiO_2 nanowires, (b) anatase nanoparticles and (c) rutile nanoparticles.

and L is the optical path length. The density of TiO_2 nanowires, anatase and rutile nanoparticles was measured to be 3.35, 3.85 and 4.25 g/cm^3, respectively.

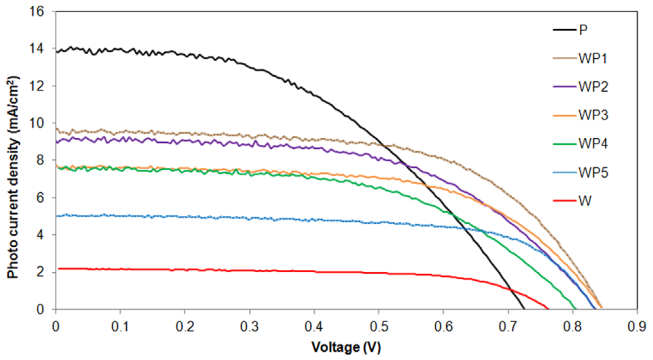

Fig. 6. Photocurrent density–voltage curve of TiO_2 solar cells with different nanowire to nanoparticle weight ratios.

The indirect band gap of nanostructures was determined by plotting $(\alpha hv)^{0.5}$ versus hv, with the extrapolation of the linear region to the low energies, being 3.35, 3.28 and 3.17 eV for TiO_2 nanowires, anatase and rutile nanoparticles, respectively. Therefore, all nanostructures displayed a blue shift relative to that of bulk TiO_2 due to the quantum confinement effect. Furthermore, TiO_2 nanoparticles showed more positive conduction band (CB) level, since their band gap energy was less than that of the nanowires. Therefore, the energy difference between the LUMO level of dye molecules and CB of TiO_2 nanoparticles was larger than that between the lowest unoccupied molecular orbital (LUMO) level of dye molecules and CB of TiO_2 nanowires, resulted in an increase of the photoelectron injection driving force (i.e., Gibbs free energy, ΔG) of nanoparticles. Consequently, a larger photocurrent was obtained for TiO_2 nanowires than that of TiO_2 nanoparticles due to possessing a lower ΔG.

3.5. Photovoltaic performance of DSSCs

3.5.1. Effect of nanowire to nanoparticle weight ratio

The photocurrent density–voltage (J–V) characteristics of fabricated TiO_2 DSSCs, with the same thickness, were illustrated in Fig. 6. In addition, the corresponding photovoltaic parameters such as short circuit current (J_{SC}), open circuit voltage (V_{OC}), fill factor (FF), adsorbed dye and power conversion efficiency (η) were summarized in Table 4.

The maximum J_{SC} was obtained for P solar cell, whereas WP1 solar cell had the highest V_{OC}. The difference in J_{SC}

Table 4
Photovoltaic parameters of TiO_2 DSSCs with different nanowire to nanoparticle weight ratios.

DSSC	V_{OC} (mV)	J_{SC} (mA/cm^2)	FF (%)	η (%)	Adsorbed dye (10^8 mol/cm^2)
P	737	13.91	47	4.69	9.41
WP1	850	9.66	60	4.89	9.04
WP2	836	9.23	56	4.25	8.71
WP3	838	7.71	61	3.91	8.35
WP4	814	7.52	56	3.33	8.01
WP5	821	5.05	67	2.79	7.69
W	782	2.71	64	1.35	4.27

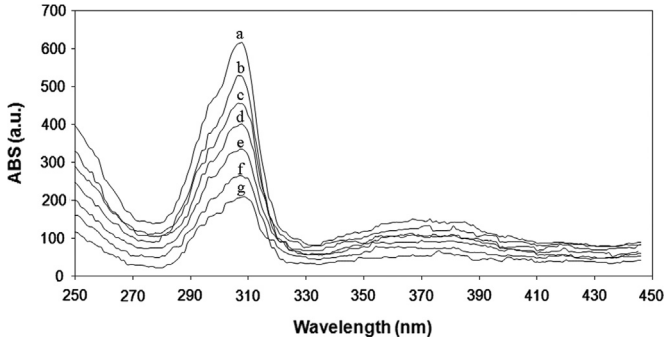

Fig. 7. Optical absorbance spectra of N719-coated TiO_2 mixed nanostructures with different nanowire:nanoparticle weight ratios: (a) P, (b) WP1, (c) WP2, (d) WP3, (e) WP4, (f) WP5 and (g) W.

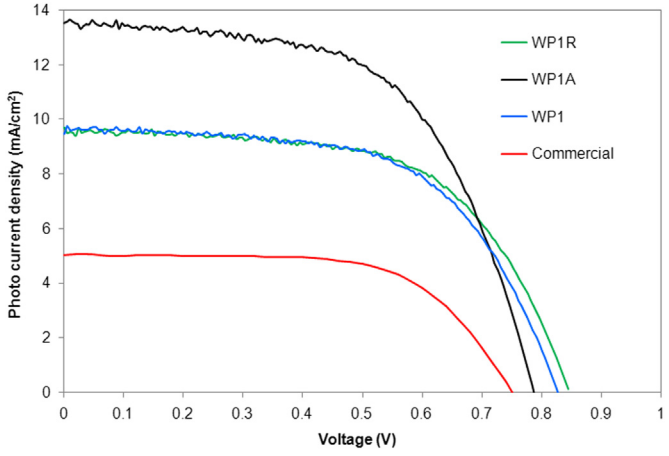

Fig. 8. Photocurrent density–voltage curve of WP1 and commercial solar cells with different nanoparticle phase composition.

of the solar cells can be related to the higher surface area of the nanoparticles compared with that of the nanowires per cell volume, resulting in greater dye sensitization of nanoparticles. The amount of adsorbed dye was determined by a spectroscopic method by measuring the concentration of desorbed dye on the titania surface into solution of 0.1 M NaOH. According to Beer–Lambert law, the amount of adsorbed dye was calculated with regards to the macroscopic geometric area of the TiO_2 electrode [31]. The absorbance of N719 dye on the P cell was found to be 2.2 times greater than that of W cell at the dye spectral maximum (310 nm), as shown in Fig. 7. Consequently, dye sensitization of the solar cells decreased with an increase of nanowire to nanoparticle weight ratio. As can be observed, the solar cell made of pure nanoparticles (i.e., P cell) had smaller V_{OC} than that of made of pure nanowire (i.e., W cell) as a result of smaller energy difference between the conductive band of nanoparticles and the iodine redox potential [32]. Furthermore, the solar cell made of W:P=50:50 (i.e., WP5 cell) showed the highest fill factor of 67% amongst all fabricated solar cells. This can be explained by the internal resistance of the cells as the most effective parameter on the fill factor. It is evident that, the power conversion efficiency of the solar cells changed with nanowire to nanoparticle weight ratio, reaching a maximum at a specific value. WP1 solar cell showed the highest power conversion efficiency of 4.89% amongst all fabricated solar cells. The improvement in the photovoltaic performance of WP1 solar cell can be explained due to its synergic effect. On one side, the nanoparticles had the highest surface area, resulting in high adsorption of dye molecules. The nanowires, on the other hand, induced improvement of light scattering and electron transport rate by multiple scattering of photons, resulting in an increase in optical path length. Consequently, a systematic design of mixed nanostructures by tailoring their phase composition and morphology can improve the photovoltaic performance of TiO_2 dye-sensitized solar cells.

3.5.2. *Effect of nanoparticle phase composition*

As described in Section 2.3, two TiO_2 solar cells containing mixtures of nanowires and as-synthesized nanoparticles with W:P=10:90 (wt%) and different phase compositions of nanoparticles (i.e., crystalline anatase and rutile phases) were prepared. One solar cell was also fabricated from commercial TiO_2 powder as a reference. The photocurrent density–voltage (J–V) characteristics of fabricated DSSCs were illustrated in Fig. 8. In addition, the corresponding photovoltaic parameters were summarized in Table 5. It is evident that, all photovoltaic parameters, except FF, of the cell made of commercial TiO_2 powder were lower than those of cells containing TiO_2 nanostructures. Furthermore, short circuit current (J_{SC}) of the cells was increased by introducing of crystalline anatase nanoparticles. The most likely reason for the enhanced J_{SC} is attributed to the increase of dye

Table 5
Photovoltaic parameters of WP1 and commercial DSSCs with different nanoparticle phase compositions.

DSSC	V_{OC} (mV)	J_{SC} (mA/cm^2)	FF (%)	η (%)	Adsorbed dye (10^8 mol/cm^2)
WP1	850	09.66	60	4.89	9.04
WP1R	824	09.47	59	4.77	8.87
WP1A	789	13.67	58	6.24	9.91
Commercial	752	05.03	63	2.41	7.35

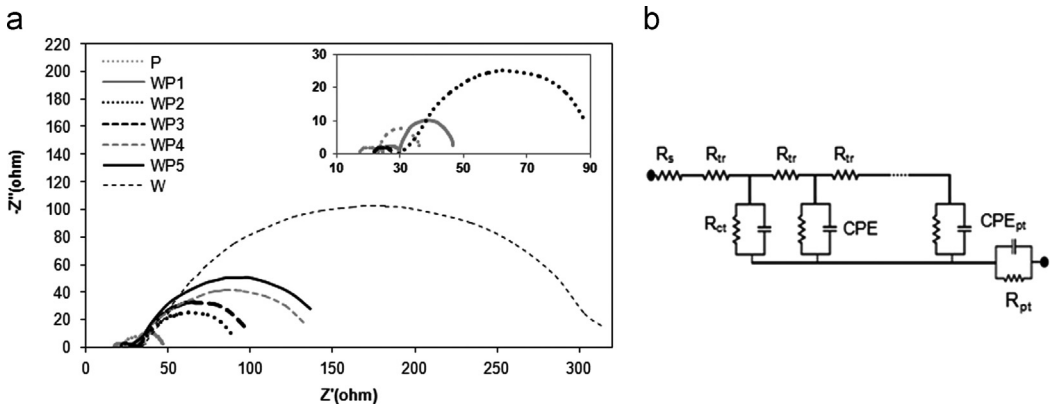

Fig. 9. Electrochemical impedance spectroscopy Nyquist plots of: (a) TiO_2 solar cells and (b) Equivalent circuits of TiO_2 DSSCs.

Table 6
Recombination and electronic transfer properties of TiO_2 cells determined by fitting EIS spectra.

Solar cell	R_s (Ω cm^2)	R_{pt} (Ω cm^2)	R_{tr} (Ω cm^2)	R_{ct} (Ω cm^2)
P	6.07	1.24	3.89	04.14
WP1	4.72	1.19	2.96	04.83
WP2	6.20	1.12	2.87	25.63
WP3	6.32	1.24	2.71	26.44
WP4	5.47	1.13	2.66	29.27
WP5	5.91	1.22	2.58	38.84
W	7.07	1.15	1.01	98.45

adsorption on TiO_2 surface. Furthermore, the solar cell contained crystalline anatase structure (i.e., WP1A) had higher power conversion efficiency and short circuit current than that made of crystalline rutile structure (i.e., WP1R). However, WP1R cell had higher V_{OC} than WP1A cell. Therefore, anatase phase is more favor than rutile phase in solar cell application due to two facts and is consistent with the result reported previously [33]. Firstly, intensity-modulated photocurrent spectroscopy and scanning electron microscopy studies indicated that electron transport was slower in the rutile layer than in the anatase layer due to differences in the extent of inter-particle connectivity associated with the particle packing density [34]. Secondly, the internal resistance of anatase crystal structure is lower than that of rutile phase due to arrangement of parallel octahedral connected by their vertices in the case of anatase compared to 90° rotated octahedral connected by their edges in the case of rutile.

3.6. Electrochemical impedance spectroscopy analysis

The internal resistance and the electron transport rate of TiO_2 DSSCs were studied using the electrochemical impedance spectroscopy (EIS). Fig. 9 shows the Nyquist plots of EIS of the cells under 100 mW/cm^2. The impedance spectra were fit to a geometrically appropriate equivalent circuit, as presented in Fig. 9c. The smaller the arc radius is, the higher the efficiency of charge separation will become [35]. All spectra can be described by three typical semicircles observed in the measured frequency at both of the nanocrystalline photoelectrodes, which are assigned to the electrochemical reaction at the Pt counter electrode (R_{pt}), charge transfer at the TiO_2/dye/electrolyte interface (R_{ct}) and Warburg diffusion process of I^-/I^{3-} (R_s) [36]. Table 6 shows recombination and electronic transfer properties of TiO_2 cells after fitting the obtained data by a proper equivalent circuit [37]. It can be observed that in

all cases the charge recombination resistance (R_{ct}) is much larger than the transport resistance (R_{tr}) which is a feature generally necessary for good performance of the DSSCs [38]. It is interesting to note that, R_{ct} was increased and R_{tr} was decreased with increasing nanowires to nanoparticle weight ratio.

Therefore, W cell showed the highest R_{ct} amongst all fabricated solar cells due to slower recapture of conduction band electrons by I^{3-} ions. Moreover, P cell had the lowest R_{ct} which indicated that the electrons were well transmitted from electrolyte to dye molecules and from dye molecules to TiO_2 film.

4. Conclusions

A systematic study of TiO_2 DSSCs by fabrication of mixed nanostructures with various morphologies (i.e., nanoparticle and nanowire) and phase composition (i.e., anatase and rutile) is presented. Such design is performed to improve the surface area, electron transport rate and the light scattering effect of the solar cells. The synthesized nanoparticles have crystallite size in the range 21–39 nm and BET surface area in the range 39.2–154.5 m^2/g depending on their crystal structure. Moreover, as-grown TiO_2 nanowires show length of several μm and diameter in the range 20–50 nm with BET surface area of 29.4 m^2/g. UV–vis analysis revealed that, TiO_2 nanowires had lower photoelectron injection driving force (ΔG) than TiO_2 nanoparticles, resulted in improvement of photocurrent of the mixed nanostructure cells. It was found that, dye sensitization of the solar cells decreased with an increase in nanowire to nanoparticle weight ratio, since the nanoparticles had higher surface area than the nanowires. However, introduction of the nanowires improved light scattering and electron transport rate by multiple scattering of photons. EIS analysis showed that, R_{ct} increased and R_{tr} decreased with increasing nanowires to nanoparticle weight ratio. The power conversion efficiency of the solar cells changed with nanowire to nanoparticle weight ratio, reaching a maximum at a specific value. An increase of 4.3% in cell efficiency was achieved by introducing 10 wt% nanowire into the as-synthesized TiO_2 nanoparticles (i.e., WP1 solar cell). It was revealed that, mixed nanostructure solar cell made of crystalline anatase nanoparticles had higher J_{SC} than that containing almost crystalline anatase nanoparticles. Furthermore, the mixed nanostructure cell (WP1) contained crystalline anatase structure had much higher power conversion efficiency and short circuit current than that made of crystalline rutile structure. An increase of 30.8% in cell efficiency was achieved by crystalline anatase phase (i.e., WP1A cell) rather than crystalline rutile structure (i.e., WP1R cell). It was concluded that, anatase phase is more favor than rutile phase in solar cell application, since the internal resistance of anatase crystal structure is lower than that of rutile phase. Finally, an increase of 27.6% in cell efficiency was achieved by crystalline anatase nanoparticles rather than the as-synthesized TiO_2 nanoparticles in WP1 solar cell (i.e., WP1A solar cell). The improved photoelectrical performance of this solar cell was attributed to the rapid transport, the less recombination of photogenerated electrons, efficient light scattering and dye adsorption. The concept of mixed nanostructure solar cells will open up new insight into fabrication and structural design of low-cost TiO_2 DSSCs with high power conversion efficiency.

Acknowledgments

The authors would like to thank the financial support from Iran Nanotechnology Initiative Council.

References

[1] J.M. Kroon, N.J. Bakker, H. Smit, P. Liska, K.R. Thampi, P. Wang, S.M. Zakeeruddin, M. Gratzel, A. Hinsch, S. Hore, U. Wurfel, R. Sastrawan, J.R. Durrant, E. Palomares, H. Pettersson, T. Gruszecki, J. Walter, K. Skupien, G.E. Tulloch, Nanocrystalline dye-sensitized solar cells having maximum performance, Progress in Photovoltaics 15 (2007) 1–18.

[2] M. Grätzel, Conversion of sunlight to electric power by nanocrystalline dye-sensitized solar cells, Journal of Photochemistry and Photobiology A 164 (2004) 3–14.

[3] Y. Chiba, A. Islam, Y. Watanabe, Dye-sensitized solar cells with conversion efficiency of 11.1%, Japanese Journal of Applied Physics 45 (2006) L638–L640.

[4] B. O'Regan, M. Grätzel, A low-cost, high-efficiency solar cell based on dye-sensitized colloidal TiO_2 films, Nature 353 (1991) 737–740.

[5] A. Hagfeldt, M. Grätzel, Light-induced redox reactions in nanocrystalline systems, Chemical Reviews 95 (1995) 49–68.

[6] M. Law, L.E. Greene, J.C. Johnson, R. Saykally, P. Yang, Nanowire dye-sensitized solar cells, Nature 4 (2005) 455–459.

[7] Q. Zhang, C.S. Dandeneau, X. Zhou, G. Cao, ZnO nanostructures for dye-sensitized solar cells, Advanced Materials 21 (2009) 1–22.

[8] X.D. Wang, Y. Ding, C.J. Summers, Z.L. Wang, Large-scale synthesis of six-nanometer-wide ZnO nanobelts, Journal of Physical Chemistry B 108 (2004) 8773–8777.

[9] K. Shankar, J.I. Basham, N.K. Allam, O.K. Varghese, G.K. Mor, X. Feng, M. Paulose, J.A. Seabold, K.S. Cho, C.A. Grimes, Recent advances in the use of TiO_2 nanotube and nanowire arrays for oxidative photoelectrochemistry, Journal of Physical Chemistry 113 (2009) 6327–6359.

[10] J.M. Wu, H.C. Shih, W.T. Wu, Formation and photoluminescence of single-crystalline rutile TiO_2 nanowires synthesized by thermal evaporation formation and photoluminescence of single-crystalline rutile TiO_2 nanowires synthesized by thermal evaporation, Nanotechnology 17 (2006) 105–109.

[11] S. Pavasupree, S. Ngamsinlapasathian, M. Nakajima, Y. Suzuki, S. Yoshikawa, Synthesis, characterization, photocatalytic activity and dye-sensitized solar cell performance of nanorods/nanoparticles TiO_2 with mesoporous structure, Journal of Photochemistry and Photobiology A 184 (2006) 163–169.

[12] K. Asagoe, S. Ngamsinlapasathian, Y. Suzuki, S. Yoshikawa, Addition of TiO_2 nanowires in different polymorphs for dye-sensitized solar cells, Central European Journal of Chemistry 5 (2007) 605–619.

[13] B. Tan, Y. Wu, Dye-sensitized solar cells based on anatase TiO_2 nanoparticle/nanowire composites, Journal of Physical Chemistry B 110 (2006) 15932–15938.

[14] C.C. Su, W.C. Hung, C.J. Lin, The Preparation of Composite TiO_2 Electrodes for Dye-sensitized Solar Cell, Journal of the Chinese Chemical Society 57 (2010) 1131–1135.

[15] K. Pan, Y. Dong, C. Tian, W. Zhou, G. Tian, B. Zhao, H. Fu, TiO_2-B narrow nanobelt/TiO_2 nanoparticle composite photoelectrode for dye-sensitized solar cells, Electrochimica Acta 54 (2009) 7350–7356.
[16] C.H. Lee, S.W. Rhee, H.W. Choi, Preparation of TiO_2 nanotube/nanoparticle composite particles and their applications in dye-sensitized solar cells, Nanoscale Research Letters 7 (2012) 48–53.
[17] T. Kasuga, M. Hiramatsu, A. Hoson, T. Sekino, K. Niihara, Titania nanotubes prepared by chemical processing, Advanced Materials 11 (1999) 1307–1311.
[18] M.R. Mohammadi, D.J. Fray, A. Mohammadi, Sol–gel nanostructured titanium dioxide: controlling the crystal structure, crystallite size, phase transformation, packing and ordering, Microporous and Mesoporous Materials 112 (2008) 392–402.
[19] S. Ito, P. Liska, P. Pechy, U. Bach, M.K. Nazeeruddin, A. Kay, S.M. Zekeeruddin, M. Grätzel, Control of dark current in photoelectrochemical ($TiO_2/I^-–I_3^-$) and dye-sensitized solar cells, Chemical Communications 34 (2005) 4351–4353.
[20] M.K. Nazeeruddin, A. Kay, I. Rodicio, R. Humphry-Baker, E. Muller, P. Liska, N. Vlachopoulos, M. Grätzel, Conversion of light to electricity by cis-X_2bis(2,2′-bipyridyl-4,4′-dicarboxylate)ruthenium(II) charge-transfer sensitizers ($X=Cl^-$, Br^-, I^-, CN^-, and SCN^-) on nanocrystalline TiO_2 electrodes, Journal of the American Chemical Society 115 (1993) 6382–6390.
[21] J.H. de Boer, B.C. Lippens, B.G. Linsen, J.C.P. Broekhoff, A. van den Heuvel, T.J. Osinga, The *t*-curve of multimolecular N_2-adsorption, Journal of Colloid and Interface Science 21 (1966) 405–414.
[22] M. Grätzel, Solar energy conversion by dye-sensitized photovoltaic cells, Inorganic Chemistry 44 (2005) 6841–6851.
[23] N. Wang, H. Lin, J. Li, L. Zhang, C. Lin, X. Li, Crystalline transition from $H_2Ti_3O_7$ nanotubes to anatase nanocrystallines under low-temperature hydrothermal conditions, Journal of the American Ceramic Society 89 (2006) 3564–3566.
[24] B.D. Cullity, S.R. Stock, in: Elements of X-ray Diffraction, third ed., Prentice Hall, Lawrence, 2001.
[25] R.A. Spurr, H. Myers, Quantitative analysis of anatase–rutile mixtures with an X-ray diffractometer, Analytical Chemistry 29 (1957) 760–761.
[26] M.R. Mohammadi, R.R.M. Louca, D.J. Fray, M.E. Welland, Dye-sensitized solar cells based on a single layer deposition of TiO_2 from a new formulation paste and their photovoltaic performance, Solar Energy 86 (2012) 2654–2664.
[27] A. Welte, C. Waldauf, C. Brabec, P. Wellmann, Application of optical absorbance for the investigation of electronic and structural properties of sol–gel processed TiO_2 films, Thin Solid Films 516 (2008) 7256–7259.
[28] D. Monllor-Satoca, R. Gomez, M. González-Hidalgo, P. Salvador, The "Direct–Indirect" model: an alternative kinetic approach in heterogeneous photocatalysis based on the degree of interaction of dissolved pollutant species with the semiconductor surface, Catalysis Today 129 (2007) 247–255.
[29] X. Chen, Titanium dioxide nanomaterials and their energy applications, Chinese Journal of Catalysis 30 (2009) 839–851.
[30] J. Tauc, in: Amorphous and Liquid Semiconductors, first ed., Plenum Press, London and New York, 1974.
[31] V. Feigenbrugel, C. Loew, S.L. Calvé, P. Mirabel, Near-UV molar absorptivities of acetone, alachlor, metolachlor, diazinon and dichlorvos in aqueous solution, Journal of Photochemistry and Photobiology A: Chemistry 174 (2005) 76–81.
[32] L. Qi, Y. Liu, C. Li, Controlled synthesis of TiO_2-B nanowires and nanoparticles for dye-sensitized solar cells, Applied Surface Science 257 (2010) 1660–1665.
[33] A.M. Bakhshayesh, M.R. Mohammadi, D.J. Fray, Controlling electron transport rate and recombination process of TiO_2 dye-sensitized solar cells by design of double-layer films with different arrangement modes, Electrochimica Acta 78 (2012) 384–391.
[34] N.G. Park, J. Vande Lagemaat, A.J. Frank, Comparison of dye-sensitized rutile- and anatase-based TiO_2 solar cells, Journal of Physical Chemistry B 104 (2000) 8989–8994.
[35] L.W. Zhang, H.B. Fu, Y.F. Zhu, Efficient TiO_2 photocatalysts from surface hybridization of TiO_2 particles with graphite-like carbon, Advanced Functional Materials 18 (2008) 2180–2189.
[36] C. Longo, J. Freitas, M.A. De Paoli, Performance and stability of TiO_2/dye solar cells assembled with flexible electrodes and a polymer electrolyte, Journal of Photochemistry and Photobiology A: Chemistry 159 (2003) 33–39.
[37] Q. Wang, S. Ito, M. Gratzel, F. Fabregat-Santiago, I. Mora-Sero, J. Bisquert, T. Bessho, H. Imai, Characteristics of high efficiency dye-sensitized solar cells, Journal of Physical Chemistry B 110 (2006) 25210–25221.
[38] A.B.F. Martinson, J.W. Elam, J.T. Hupp, M.J. Pellin, ZnO nanotube based dye-sensitized solar cells, Nano Letters 7 (2007) 2183–2187.